IEEE Access
Multidisciplinary | Rapid Review | Open Access Journal

Received December 2, 2017, accepted December 25, 2017, date of publication January 8, 2018, date of current version March 9, 2018.

Digital Object Identifier 10.1109/ACCESS.2018.2789981

Color Transfer Using Adaptive Second-Order Total Generalized Variation Regularizer

BIN XIE[1,2], CHEN XU[1], YU HAN[3], AND ROBERT K. F. TENG[1]

[1]College of Information Engineering, Shenzhen University, Shenzhen 518060, China
[2]College of Information Engineering, Jiangxi University of Science and Technology, Ganzhou 341000, China
[3]College of Mathematics and Statistics, Shenzhen University, Shenzhen 518060, China

Corresponding author: Chen Xu (xuchen_szu@163.com)

This work was supported in part by the National Natural Science Foundation of China under Grant 61402290, Grant 61472257, Grant 61772343, and Grant 61379030; in part by the Foundation for Distinguished Young Talents in Higher Education of Guangdong, China, under Grant 2014KQNCX134; in part by the Natural Science Foundation of Guangdong, China, under Grant 1714050003822; and in part by the Science Foundation of Shenzhen Science Technology and Innovation Commission, China, under Grant JCYJ20160331114526190.

ABSTRACT Color transfer is to generate synthetic images by changing the color of target images with new colors obtained from given source images, while the geometrical structure of the synthetic images remains the same. Classical color transfer models use a total variation (TV) regularizer to preserve the details and suppress the noise of the synthetic images. These models can sometimes cause staircase effect and geometrical structure details over-smoothed. To overcome these problems, we propose a new color transfer model in which an adaptive second-order total generalized variation (TGV) regularizer is designed. Here, the adaptive second-order TGV regularizer is a weighted second-order TGV regularizer. The weight is computed by an adaptive edge indicator function. In addition, an efficient algorithm is developed to program our new model. The algorithm is based on a weighted primal–dual method. Experimental results and comparisons demonstrate that our new color transfer model can generate better results than classical TV regularizer-based models in the aspects of the inhibition of staircase effect and the preservation of image details.

INDEX TERMS Color transfer, staircase effect, total variation (TV), total generalized variation (TGV), primal-dual algorithm.

I. INTRODUCTION

Color transfer is a technique that the color information of input ''source images'' can be transferred to input ''target images.'' The newly synthetic images are usually called as ''resulting images.'' Here, the resulting images not only keep the structural information of the target images, but also have the color information of the source images. The technique of color transfer has important application in film editing, computer animation, medical image colorization, color correction and so on [1]–[4]. In recent years, color transfer has attracted a lot of attention of the researchers [4]–[10]. Reinhard *et al.* [1] originally propose a color transfer method based on the statistical characteristics of images. The method in [1] is fast and simple, but to some extent, it produces unnatural results when images to be processed have different color distributions. Since then, various kinds of color transfer methods are springing up constantly. Existing color transfer methods mainly include local methods [2]–[7] and global methods [11]–[14].

Local methods usually achieve the purpose of color transfer by local feature matching between images. A stroke based color transfer method of gray images is proposed by Levin *et al.* [2]. In the approach, the users are requested to stroke the fond colors in different interior zones of images. A local color transfer method based on EM (Expectation-Maximization) scheme and color smoothness is proposed by Tai *et al.* [3], and good effect of regional color transfer between two images is realized by soft color segmentation. To further improve the performances of the methods in [2] and [3], Chang *et al.* [4] propose a color transfer scheme based on user-modified palette. In the method, the users can recolor images according to their own interests, and the color transfer results are related to the subjective consciousness of users. Han *et al.* [5] propose to use the concept of color theme to simulate consciousness of users and propose a cartoon-and-texture decomposition based local color transfer approach. There are two sequential phases in the approach. In the first phase, an input image is decomposed

into its cartoon and texture components. During the decomposition process, the cartoon component is simultaneously segmented into several regions. In the second phase, a new cartoon component is generated by transferring the colors in a given color theme. Then, resulting images can be reconstructed by integrating the new cartoon component and the original texture component. In general, the traditional local color transfer methods usually need to use some subjective interventions or some image segmentation algorithms if they want to obtain good effect. Then, it may aggravate the burdens of users when the images have complex textures and patterns. In addition, deep neural networks [8]–[10] are also used in achieving local color transfer. For example, Yan *et al.* [8] propose that the local semantics of source images are used to produce image descriptors, and resulting images can be generated by learning the descriptors. Although deep neural network based methods can obtain relatively good results, they tend to be time-consuming since the number of training samples is usually very large, and the structures of learning networks are usually complicated.

For the global color transfer methods, global information of the source images and the target images are taken into account. The global methods can automatically perform the task of color transfer and greatly reduce the subjectivity and the uncertainty of manual interventions. In this sense, the global color transfer methods have higher application value. In [13], an automatic, global color transfer algorithm of grayscale images is proposed by Welsh *et al.* In the approach, color transfer is realized by matching the luminance information between source images and target images. Xiao and Ma [14] propose an improved algorithm on the basis of Reinhard's algorithm. Xiao's algorithm gets the color matching scheme by using the correlation of image covariance. Xu *et al.* [15] propose a novel color tone matching scheme based on region-of-interests (ROIs). In the method, global tone mapping curves are created by analyzing features from multiple ROIs, and good visual experience is achieved under the guidance of the tone mapping curves. Chen *et al.* [16] follow the work [15] and introduce an intra-and-inter-frame constraint to achieve color transfer of videos. Sun *et al.* [17] propose a weighted Mahalanobis distance to achieve color matching on the statistics of mean and variance in the YUV color space. However, resulting images obtained from above methods may have defects such as noise enhancement since data noise influences matching processes. In order to solve the problem, variational framework [18], [19] has been introduced in some color transfer methods [20]–[24] in recent years. In particular, among these variational based methods, the TV regularizer [22]–[24] becomes very popular in color transfer due to the anisotropy characteristics of the TV regularizer [25], [26]. Rabin and Peyré [22] propose a classical color transfer method, which combines the TV regularizer and the Wasserstein distance. The method can simultaneously perform color matching and its regularization by a method of variational energy minimization. Feng *et al.* [23] follow Rabin's model and propose to use a color wheel to guide the process of color matching. Bugeau *et al.* [24] further introduce a spatial constraint into TV regularizer based model to obtain better color transfer results.

Although the TV regularizer plays a valuable role in above methods, there still have two problems due to the use of the TV regularizer. Problem One: the function space of the TV regularizer has piecewise smooth feature which is easy to produce staircase effect [27], [28]. Then, the quality of the resulting images will be severely impacted by the staircase effect. How to restrain the staircase effect is a very important problem in color transfer. Problem Two: some small details may be over-smoothed, and it will lead to the fuzzy phenomenon of the resulting images [29], [30]. Then, the color transfer results will produce certain flaws. In order to solve Problem One, we introduce the second-order TGV [31] of image as the regularizer term in this paper. The second-order TGV can automatically balance the relation between the first derivative term and the second derivative term according to image characteristics, and it can restrain the staircase effect better [31], [32]. For convenience, we use the TGV to represent the second-order TGV in subsequent content. We should note that the TGV has been also used in Han's local color transfer method [5] to remove the staircase effect in image decomposition processes. In this paper, we follow the work [5] and introduce the TGV in achieving global color transfer. Although the TGV is good at restraining staircase effect, the ability of preserving image details of TGV is limited [30]. For solving Problem Two, we design an adaptive edge indicator function which can enhance the ability of preserving image details of our model.

In summary, in this paper we propose a new global color transfer method based on adaptive TGV regularizer. Comparing with classical global color transfer methods based on TV regularizer, our method has following primary innovations. Firstly, we introduce the TGV regularizer to restrain the staircase effect which is usually produced in the TV regularizer based methods. As described in [33] and [34], the TGV regularizer can effectively restrain staircase effect and noise, and it is very suitable for solving the optimization problem. Secondly, to preserve the details of the resulting images better, we design a TGV regularizer with an adaptive edge indicator function. Our color transfer method can effectively protect the details of the resulting images under the action of the adaptive edge indicator function. Moreover, we design a new numerical algorithm based on weighted primal-dual algorithm to efficiently solve our model.

II. RELATED WORK AND DISCUSSION

A. CLASSICAL TV REGULARIZER BASED COLOR TRANSFER MODEL

In [22], a classical TV regularizer based color transfer model is proposed by Rabin *et al.* Let $\chi : \chi_i = (\chi_R(i), \chi_G(i), \chi_B(i))^T \in \Gamma(i \in \Omega)$ be a discrete color image with RGB format, where $\Omega \subset \mathbb{Z}^2$ denotes the spatial domain which include κ pixels, and $\Gamma \subset \mathbb{R}^3$ is the RGB color cube.

Let g be a target image, h be a source image, and d be a resulting image. Both the target image and the source image are input by users, and d is under-estimated. The target image (resp. the source image) is used to provide the structural information (resp. the color information) for the resulting image. In Rabin's model, the task of color transfer is equivalent to obtain d^*, the solution of the following optimization problem:

$$d^* = \arg\min_d \{\lambda_W W_2(d,h) + \lambda_R R(d) + F(d,g)\}, \quad (1)$$

where $W_2(d,h)$ is a color penalty term based on the quadratic Wasserstein distance [35], [36], $R(d)$ is the TV regularizer, $F(d,g)$ is called as the fidelity term, and λ_W and λ_R are two positive tuning parameters. Below, we give more discussion on each term of model (1).

In model (1),

$$W_2(d,h) = \min_{\sigma \in \sum(\Omega)} \left\{ \sum_{i\in\Omega} \sum_{j\in\{\mathrm{R,G,B}\}} \left\| d_{ji} - h_{j\sigma(i)} \right\|_2^2 \right\}, \quad (2)$$

where $\|\cdot\|_2$ is the classical l_2 norm, $\sigma \in \sum(\Omega)$, and $\sum(\Omega)$ is the set of all permutations of Ω. Eq. (2) is the definition of the Wasserstein distance between d and h, when σ is the optimal permutation. Eq. (2) can be used to penalize the color distribution differences between the resulting image d and the source image h in model (1). It is worth noting that, for the reason $W_2(d,h)$ is hard to be computed directly, in [22] $W_2(d,h)$ is approximated by a sliced Wasserstein distance. In this paper, we follow the work [22] to use the sliced Wasserstein distance in our image color transfer model. For convenience, the notation $W_2(d,h)$ mentioned below refers to the sliced Wasserstein distance between d and h.

The TV regularizer term $R(d)$ in model (1) is defined as

$$R(d) = \sum_{j\in\{\mathrm{R,G,B}\}} \left\| |\nabla d_j| \right\|_1 = \sum_{j\in\{\mathrm{R,G,B}\}} \sum_{i\in\Omega} \sqrt{(\partial_x d_{ji})^2 + (\partial_y d_{ji})^2}, \quad (3)$$

where $d = (d_\mathrm{R}, d_\mathrm{G}, d_\mathrm{B})^T$, $\nabla = (\partial_x, \partial_y)^T$ is the gradient operator, $|\nabla d_j|$ is the module of ∇d_j, and $\|\cdot\|_1$ is the l_1 norm. According to Eq. (3), the term $R(d)$ in model (1) makes the estimated image d smoother than the image g since some noisy geometrical structure details of the image g can be removed through minimizing the term $R(d)$.

The fidelity term $F(d,g)$ in model (1) consists of the following two parts,

$$\begin{aligned} F(d,g) &= Z(d,g) - \lambda_T B(d,g) \\ &= \|d-g\|_2^2 - \lambda_T \left\langle \nabla d, \frac{\nabla g}{\||\nabla g|\|_1} \right\rangle, \end{aligned} \quad (4)$$

where λ_T is a positive tuning parameter. In Eq. (4),

$$Z(d,g) = \|d-g\|_2^2, \quad (5)$$

and

$$B(d,g) = \left\langle \nabla d, \frac{\nabla g}{\||\nabla g|\|_1} \right\rangle. \quad (6)$$

Both of the two terms in $F(d,g)$ can ensure the resulting image d and the target image g containing similar image details. In fact, when $F(d,g)$ is minimized, the image d is approximated to the image g, which can make d and g having similar geometrical structure information. At the same time, the gradient ∇d is approximately parallel to the normal direction of g, $\nabla g / \||\nabla g|\|_1$, which can also keep the details in the image d similar to the ones in the image g.

Although the above TV regularizer based color transfer model can obtain relatively good results, the TV regularizer has two main disadvantages. It tends to produce staircase effect in color transfer results, and it tends to oversmooth some important image details. For example, Fig. 1 shows a color transfer result obtained from the TV regularizer based model in [22]. Fig. 1 (a), (b) and (c) are a source image, a target image and a resulting image, respectively. Fig. 1 (d) and (f) are two local enlarged parts of Fig. 1 (b). Corresponded to Fig. 1 (d) and (f), Fig. 1 (e) and (g) are two local enlarged color transfer results shown in Fig. 1 (c).

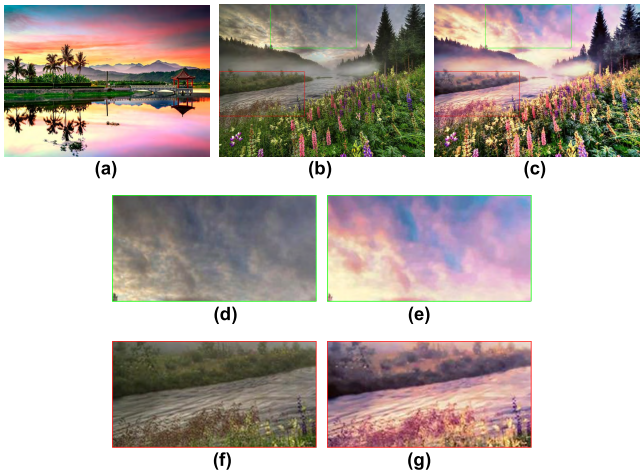

FIGURE 1. The TV regularizer based color transfer results obtained from the work in [22]. (a), (b) and (c) are a source image, a target image and a resulting image, respectively, (d) (resp. (e)) is the local enlarged part of the green box marked in (b) (resp. (c)), and (f) (resp. (g)) is the local enlarged part of the red box marked in (b) (resp. (c)).

From the result shown in Fig. 1 (e), we can find that the cloud scene has staircase effect since the colors of the corresponding scene in Fig. 1 (d) varies homogeneously. Moreover, from the result shown in Fig. 1 (g), we can find that some image details are over-smoothed comparing with the corresponding scene in Fig. 1 (f). Then, according to the results shown in Fig. 1, although the color transfer method in [22] can well retain most geometrical structure details of the target image in the resulting image and can well suppress noisy image details, the method tends to produce staircase effect and tends to oversmooth some image details due to the TV regularizer. To overcome these drawbacks, in this paper an adaptive TGV regularizer is introduced.

B. THE TGV REGULARIZER

To restrain the staircase effect which is usually brought by the TV regularizer in image restoration, Bredies *et al.* [31]

proposed the TGV regularizer. Proved in [31], the first-order TGV regularizer is equivalent to the original TV regularizer. The second-order or higher-order TGV regularizer can remove the staircase effect of restored images. However, too high-order TGV regularizers are relatively hard to implement. Therefore, as mentioned in Section I, we only focus on the second-order TGV regularizer in this paper, and, below, we refer the TGV regularizer in particular to be the second-order TGV regularizer. The TGV regularizer on a color image d is defined as follows,

$$TGV_{\alpha}^{2}(d) = \min_{e\in BD^{3}(\Omega)} \left\{ \sum_{j\in\{\mathrm{R,G,B}\}} \alpha_{1j} \left\| \nabla d_j - e_j \right\|_1 + \alpha_{0j} \left\| \varepsilon(e_j) \right\|_1 \right\}, \tag{7}$$

where $e = (e_{\mathrm{R}}, e_{\mathrm{G}}, e_{\mathrm{B}})^T$, $\varepsilon(e_j) = (\nabla e_j + \nabla e_j^T)/2$ is the symmetrized derivative on e_j, ∇e_j^T is the transportation of ∇e_j, and $\alpha_{0j} > 0$, $\alpha_{1j} > 0$ are two tuning parameters. The denotation $BD(\Omega)$ is the so-called bounded and distorted space of vector fields [31], and $BD^3(\Omega) = BD(\Omega) \times BD(\Omega) \times BD(\Omega)$.

From Eq. (7), we can find that the TGV regularizer can automatically balance the relation between the first derivative constraint $e_j \approx \nabla d_j$ and the second derivative constraint $\nabla e_j + \nabla e_j^T \approx 0$. This is the main reason why the TGV regularizer can remove the staircase effect from restored images [37], [38]. Inspired by the image restoration work in [31], we introduce an adaptive TGV regularizer in our new color transfer model. The adaptive TGV regularizer can better preserve image details than the original TGV regularizer.

III. THE PROPOSED MEDEL

In order to restrain the staircase effect and to preserve the details of the resulting image, we propose a new color transfer model based on an adaptive TGV regularizer. Our new color transfer model can be expressed as follows,

$$\hat{d} = \arg\min_{d} \left\{ Z(d, g) + \lambda_W W_2(d, h) + ATGV_{\alpha}^{2}(d) \right\}, \tag{8}$$

where $Z(d, g)$ is a fidelity term whose goal is to keep that the structural information in a resulting image d is consistent with that in a target image g, $W_2(d, h)$ is a quadratic Wasserstein distance between the resulting image d and a source image h, which is also used in model (1), λ_W is a tuning parameter, $ATGV_{\alpha}^{2}(d)$ is our newly designed adaptive TGV regularizer, and $\hat{d}$ is our final optimal color transfer resulting image. Below, we give a discussion on our model (8) in details.

A. A SIMPLER FIDELITY TERM

The fidelity term in our model (8), $Z(d, g)$, is a special case of $F(d, g)$ in model (1) when the tuning parameter λ_T is set to be zero. In fact, according to the discussion in Section II Part A, both $Z(d, g)$ and $B(d, g)$ are good at preserving image details. However, the term $B(d, g)$ can produce some negative impacts on color transfer results, especially when λ_T is set to be relatively large values. For example, in Fig. 2, we compare different resulting images obtained from model (1) with $\lambda_T = 0$, 0.06, 0.3, 1.5 and 3, respectively, while keeping $\lambda_W = 15$ and $\lambda_R = 0.0002$. Fig. 2 (a)-(e) correspond to $\lambda_T = 0$, 0.06, 0.3, 1.5 and 3, respectively, (f)-(i) correspond to the differences between (a) and (k) (k = b, c, d and e), respectively. Here, the source image and the target image are still the images shown in Fig. 1 (a) and (b), respectively.

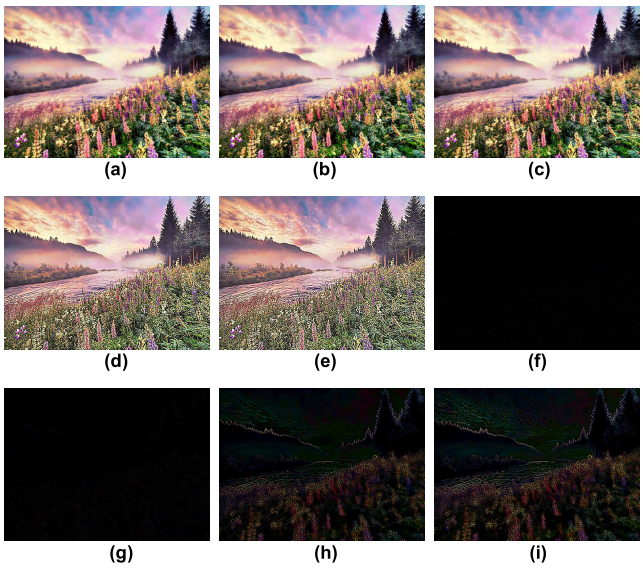

FIGURE 2. The comparison of the color transfer results obtained from model (1) with different λ_T. (a)-(e) correspond to $\lambda_T = 0$, 0.06, 0.3, 1.5 and 3, respectively, (f)-(i) correspond to the differences between (a) and (k) (k = b, c, d and e), respectively.

From the results shown in Fig. 2, we can find that the colors of (a), (b) and (c) are all brighter and fuller than (d) and (e) , while the results shown in (d) and (e) seem not only unnaturally overexposed, but also bleak and withered. Furthermore, it is hard to distinguish the differences among (a), (b) and (c). In fact, as shown in Fig. 2 (f) (resp. Fig. 2 (g)), the differences between Fig. 2 (a) and Fig. 2 (b) (resp. between Fig. 2 (a) and Fig. 2 (c)) are not quite obvious in vision. It demonstrates that, although larger λ_T can promise the preservation of image details, model (1) tends to obtain relatively better color transfer results only when $\lambda_T$is small enough. Then, to ensure the effectiveness of color transfer, in our model (8) we set $\lambda_T = 0$ and use the term $Z(d, g)$ to preserve the details of resulting images.

B. AN ADAPTIVE TGV REGULARIZER TERM

The adaptive TGV regularizer on the resulting image d in our model (8) is given by

$$ATGV_{\alpha}^{2}(d) = \min_{e\in BD^{3}(\Omega)} \left\{ \sum_{j\in\{\mathrm{R,G,B}\}} \alpha_{1j} A(d_j) \left\| \nabla d_j - e_j \right\|_1 + \alpha_{0j} \left\| \varepsilon(e_j) \right\|_1 \right\}, \tag{9}$$

where $d = (d_R, d_G, d_B)^T$, and $A(d_j)(j \in \{R,G,B\})$ is our newly defined adaptive edge indicator for each color channel, namely,

$$A(d_j) = \frac{1}{1 + \sigma_j \left\| \nabla d_j \right\|_1^2}. \tag{10}$$

Here, $\sigma_j \geq 0$ is a tuning parameter. From Eq. (10), we can find that $A(d_j) \approx 0$ when $\left\| \nabla d_j \right\|_1$ is large, and $A(d_j) \approx 1$ when $\left\| \nabla d_j \right\|_1 \approx 0$. It demonstrates that the function $A(d_j)$ is an adaptive edge indicator [23] for the corresponding color channel of the image d.

The introduction of the edge indicator $A(d_j)$ in the TGV regularizer is to further protect the details of the image d. In fact, for the case $A(d_j) \approx 0$, Eq. (9) shows that a pixel point i of d_j is an edge point, and the direction of ∇d_jat point i is not needed to be rigidly paralleled to e_j. It means that our model (8) can drive d_j at point i not to be smoothed as the way of the case $A(d_j) \approx 1$. Then, the details of the image d can be protected.

C. THE SOLUTION OF OUR MODEL

In order to solve our color transfer model (8) efficiently, we design a new algorithm in which both the former-backward operator splitting method [39] and the primal-dual method [40] are used. Here, the former-backward operator splitting method is to obtain the solution of model (8), $\hat{d}$, by an iteration process. More specifically, starting from a given initialization, $d^{(0)} = g$, the minimization problem (8) is converted into the following forward-backward iteration which includes a gradient descent step (11) and a proximal correction step (12) :

$$\tilde{d}^{(t)} = d^{(t-1)} - \tau \nabla [Z(d^{(t-1)}, g) + \lambda_W W_2(d^{(t-1)}, h)], \tag{11}$$

$$d^{(t)} = \text{prox}_{\tau ATGV}(\tilde{d}^{(t)}), \tag{12}$$

where t is the iteration index, $t = 1, 2, 3, \cdots$, and τ is an iteration step. The stopping criterion of the algorithm is to meet the following condition,

$$\frac{\left\| d^{(t)} - d^{(t-1)} \right\|_2^2}{\left\| d^{(t)} \right\|_2^2} \leq \xi, \tag{13}$$

where ξ is a threshold for the stopping criterion. In our experiments, we use $\xi = 10^{-6}$. When the condition of the stopping criterion is met, the final optimal color transfer resulting image $\hat{d} = d^{(t)}$ with t iterations. Note that the iteration process shown in Eq. (11) and Eq. (12) is similar to the one designed by Rabin and Peyré [22]. However, the difference between our iteration process and the iteration given in [22] lies in Eq. (12). More precisely, in Eq. (12), the operator $\text{prox}_{\tau ATGV}$ is equivalent to a newly proposed weighted TGV minimization problem as follows,

$$d^{(t)} = \arg\min_u \left\{ \frac{1}{2} \left\| u - \tilde{d}^{(t)} \right\|_2^2 + ATGV_\alpha^2(u) \right\}, \tag{14}$$

where $d^{(t)} = (d_R^{(t)}, d_G^{(t)}, d_B^{(t)})^T$. In actual computation, we can simply assume that different color channels are independent with each other. Then, the minimization problem (14) can be respectively minimized for each of the color channels R, G and B. Furthermore, combining the expression of $ATGV_\alpha^2(u)$, the minimization problem (14) can be transferred into the following equivalent form in each color channel,

$$\min_{u_j, e_j} \left\{ \frac{1}{2} \left\| u_j - \tilde{d}_j^{(t)} \right\|_2^2 + \alpha_{1j} A(u_j) \left\| \nabla u_j - e_j \right\|_1 + \alpha_{0j} \left\| \varepsilon(e_j) \right\|_1 \right\}, \tag{15}$$

where $j \in \{R,G,B\}$. The minimization problem (15) is still difficult to be solved since the term $A(u_j) \left\| \nabla u_j - e_j \right\|_1$ is non-convex with respect to u_j. To overcome the difficulty, we simply set the edge indicator $A(u_j) = A(\tilde{d}_j^{(t)})$, and then we have the following minimization problem,

$$\min_{u_j, e_j} \left\{ \frac{1}{2} \left\| u_j - \tilde{d}_j^{(t)} \right\|_2^2 + \alpha_{1j} A(\tilde{d}_j^{(t)}) \left\| \nabla u_j - e_j \right\|_1 + \alpha_{0j} \left\| \varepsilon(e_j) \right\|_1 \right\}. \tag{16}$$

For the minimization problem (16), it is convex on u_j and e_j, respectively. Then, we can use some efficient convex optimization algorithms to solve the minimization problem (16). Considering that the minimization problem (16) corresponds to a special image denoising problem discussed by Xu *et al.* [38], in this paper we follow Xu's work to solve the minimization problem (16), and a new weighted primal-dual algorithm is proposed. The weighted primal-dual algorithm is a generalized version of the original primal-dual algorithm in [40], and the original primal-dual algorithm has been well studied in the field of image processing [41]–[45].

According to the primal-dual theory, the dual problem of Eq. (16) is listed as follows,

$$\min_{u_j, e_j} \max_{p_j \in P_j, q_j \in Q_j} \left\{ \langle \nabla u_j - e_j, p_j \rangle - F_1^*(p_j) + \langle \varepsilon(e_j), q_j \rangle - F_2^*(q_j) + \frac{1}{2} \left\| u_j - \tilde{d}_j^{(t)} \right\|_2^2 \right\}, \tag{17}$$

where

$$F_1^*(p_j) = \begin{cases} 0, & |p_j| \leq \alpha_{1j} A(\tilde{d}_j^{(t)}) \\ +\infty, & |p_j| > \alpha_{1j} A(\tilde{d}_j^{(t)}), \end{cases}$$

$$F_2^*(q_j) = \begin{cases} 0, & |q_j| \leq \alpha_{0j} \\ +\infty, & |q_j| > \alpha_{0j}, \end{cases}$$

$$P_j = \left\{ p_j = (p_{1j}, p_{2j})^T \,\middle|\, \left\| p_j \right\|_\infty \leq \alpha_{1j} A(\tilde{d}_j^{(t)}) \right\}$$

and

$$Q_j = \left\{ q_j = \begin{bmatrix} q_{j11} & q_{j12} \\ q_{j21} & q_{j22} \end{bmatrix} \,\middle|\, \left\| q_j \right\|_\infty \leq \alpha_{0j} \right\}.$$

Then, the minimization problem (17) can be solved by the iteration process listed in Algorithm 1.

In Algorithm 1, s is the iteration index, $div^\hbar = -\varepsilon^*$ is the negative conjugate of symmetrical gradient operator ε, $\text{proj}_{P_j}(p_j) = \frac{p_j}{\max(1, \frac{|p_j|}{\alpha_{1j} A(\tilde{d}_j^{(t)})})}$, and $\text{proj}_{Q_j}(q_j) = \frac{q_j}{\max(1, \frac{|q_j|}{\alpha_{0j}})}$.

Algorithm 1 The Weighted Primal-Dual Algorithm for the Minimization Problem (17)

Initialize: $u_j^{(0)} = \bar{u}_j^{(0)} = \tilde{d}_j^{(t)}$, $e_j^{(0)} = \bar{e}_j^{(0)} = 0^*$, $p_j^{(0)} = q_j^{(0)} = 0$, $s = 0$, $\gamma_j, \tau_j, \alpha_{1j}, \alpha_{0j} > 0$.

Repeat:

1. $p_j^{(s+1)} = \mathrm{proj}_{P_j}[p_j^{(s)} + \gamma_j(\nabla \bar{u}_j^{(s)} - \bar{e}_j^{(s)})]$;
2. $q_j^{(s+1)} = \mathrm{proj}_{Q_j}[q_j^{(s)} + \gamma_j(\varepsilon(\bar{e}_j^{(s)}))]$;
3. $u_j^{(s+1)} = \frac{u_j^{(s)} + \tau_j div(p_j^{(s+1)}) + \tau_j \tilde{d}_j^{(t)}}{1+\tau_j}$;
4. $e_j^{(s+1)} = e_j^{(s)} + \tau_j[p_j^{(s)} + div^{\hbar}(q_j^{(s+1)})]$;
5. $\bar{u}_j^{(s+1)} = 2u_j^{(s+1)} - u_j^{(s)}$;
6. $\bar{e}_j^{(s+1)} = 2e_j^{(s+1)} - e_j^{(s)}$;
7. $s = s + 1$;

Until: the constraint $\frac{\left\|u_j^{(s+1)} - u_j^{(s)}\right\|_2^2}{\left\|u_j^{(s)}\right\|_2^2} \leq 10^{-6}$ is satisfied, and then output $d_j^{(t)} = u_j^{(s+1)}$, otherwise return to 1.

IV. NUMERICAL EXPERIMENTS AND ANALYSIS

In this section, to demonstrate the effectiveness of our new method, we present several typical color transfer results on some images with different styles. The results are also compared with the ones obtained from the TV regularizer based method in [22] and the original TGV regularizer based method. For the sake of convenience, the TV regularizer based color transfer method in [22] is simply referred to be the TV-CT method, the original TGV regularizer based color transfer method is referred to be the OTGV-CT method, and our newly proposed method is referred to be the ATGV-CT method, which represents the adaptive TGV regularizer based color transfer method.

To make readers more intuitively understand the performance of our ATGV-CT method, Fig. 3 and 4 show two sets of color transfer results with the target images respectively called as "stone bridge in winter" and "morning mist." Here, the sizes of the images are 800 × 600. In Fig. 3 and 4, (a) and (b) are the source image and the target image, respectively, (c) and (d) are the resulting images obtained from the TV-CT method and our ATGV-CT method, respectively, and (e) (resp. (f) and (g)) is the local enlarged part of (b) (resp. (c) and (d)).

From the results shown in Fig. 3 (f) and (g) (resp. Fig. 4 (f) and (g)), we can find that, comparing with the corresponding scene in Fig. 3 (e) (resp. Fig. 4 (e)), the resulting image obtained from the TV-CT method is over-smoothed and has staircase effect, while the resulting image obtained from our ATGV-CT method overcomes the above drawbacks well. Moreover, the geometrical structure details of the original target image are better maintained. It proves that it is necessary for our color transfer model to introduce the adaptive TGV regularizer.

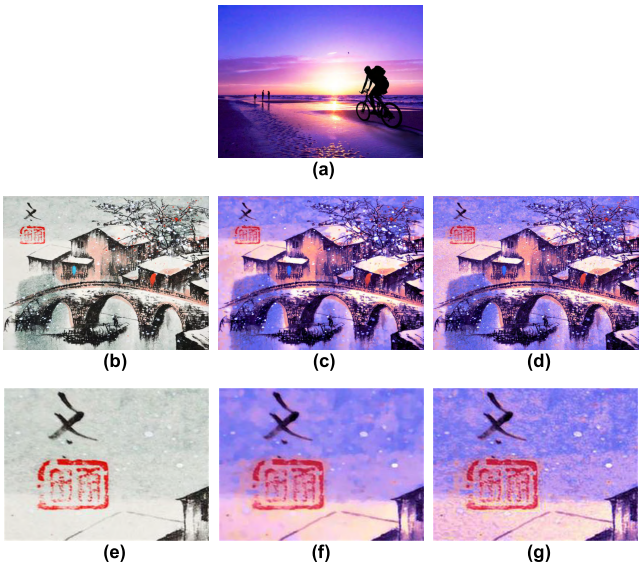

FIGURE 3. The color transfer results with the target image called as "stone bridge in winter." (a) is the source image, (b) is the target image, (c) (resp. (d)) is the resulting image obtained from the TV-CT method (resp. our newly proposed ATGV-CT method), and (e) (resp. (f) and (g)) is the local enlarged part of (b) (resp. (c) and (d)).

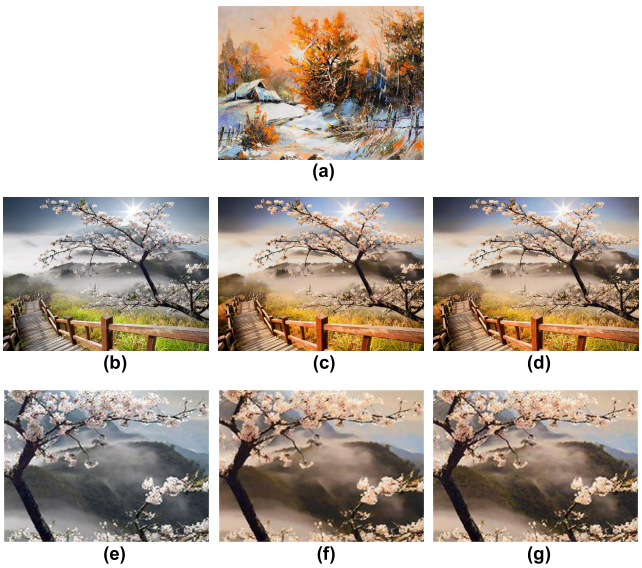

FIGURE 4. The color transfer results with the target image called as "morning mist." (a) is the source image, (b) is the target image, (c) (resp. (d)) is the resulting image obtained from the TV-CT method (resp. our newly proposed ATGV-CT method), and (e) (resp. (f) and (g)) is the local enlarged part of (b) (resp. (c) and (d)).

A. THE SELECTION OF PARAMETERS

In this section, we focus on the main parameters of our ATGV-CT method. The example shown in Fig. 3 is used to explain the selection of the parameters in our ATGV-CT method. As mentioned in Section III Part C, in order to solve our newly proposed model (8), we divide it into Eq. (11) and Eq. (12) by the former-backward operator splitting method. Eq. (11) can be easily solved by the gradient descent method.

By testing, we find that the step length τ of the gradient descent method can be simply fixed to be 0.1. In addition, Eq. (12) is equivalent to a special image denoising problem (16) whose parameters include α_{0j}, α_{1j} and $\sigma_j (j \in \{R,G,B\})$. In general, the noise for images used in the process of color transfer is relatively small. Therefore, the model (16) can be approximately regarded as a weighted TGV denoising model under the background of small noise. The selection of the above three parameters can be conveniently obtained by using triple optimization. Through a large number of experiments, we find that α_{0j}, α_{1j} and $\sigma_j (j \in \{R,G,B\})$ can be simply fixed to be 0.0012, 0.0006 and 2.6, respectively. In order to test the tuning parameter λ_W of model (8), we introduce two evaluation indexes *ERRJ* and *ERRI* as follows,

$$ERRJ = \frac{\left\|d^{(t)} - d^{(t-1)}\right\|_2^2}{\left\|d^{(t)}\right\|_2^2}, \tag{18}$$

and

$$ERRI = \frac{\left\|d^{(t)} - g\right\|_2^2}{\left\|d^{(t)}\right\|_2^2}. \tag{19}$$

In Eq. (18), $d^{(t)}$ (resp. $d^{(t-1)}$) denotes the resulting image obtained from our ATGV-CT method after t(resp.$t-1$) time forward-backward iterations, and the convergence state of our color transfer algorithm can be indicated by the evaluation index *ERRJ*. In Eq. (19), g is the target image, and $d^{(t)} - g$ denotes the difference between the target image and the resulting image obtained after t time forward-backward iterations. Then, the effect of our color transfer algorithm can be indicated by the evaluation index *ERRI*. Fig. 5 shows the influence of different λ_W on our iteration processes. Fig. 5 (a) (resp. (b)) is the curves of *ERRJ* (resp. *ERRI*) of our color transfer results shown in Fig. 3, for different choices of the tuning parameter λ_W with the iteration index t increasing.

From the curves shown in Fig. 5, we can find that, for the case $\lambda_W \leq 15$, the *ERRJ* index rapidly decreases and tends to be zero with the iteration index t increasing, and the *ERRI* index gradually increases and tends to be a stable level with the iteration index t increasing. It demonstrates that the resulting images obtained from our ATGV-CT method are stable when $t \geq 15$. Moreover, through a large number of experiments, we find that both the *ERRJ* index and the *ERRI* index fluctuate constantly with the iteration index t increasing when $\lambda_W \geq 20$, which means the results of color transfer are not robust for $\lambda_W \geq 20$. So, in order to guarantee the stability of our new model, the condition $\lambda_W \leq 15$ needs to be satisfied.

Furthermore, in Fig. 6 (a)-(d), we compare different resulting images obtained from our model (8) with $\lambda_W = 1$, 5, 10 and 15, respectively. Here, we also use the source image (resp. the target image) shown in Fig. 3 (a) (resp. (b)). From the results shown in Fig. 6, we can find that the color information of the resulting image are more and more close to those of the source image with the tuning parameter λ_W increasing.

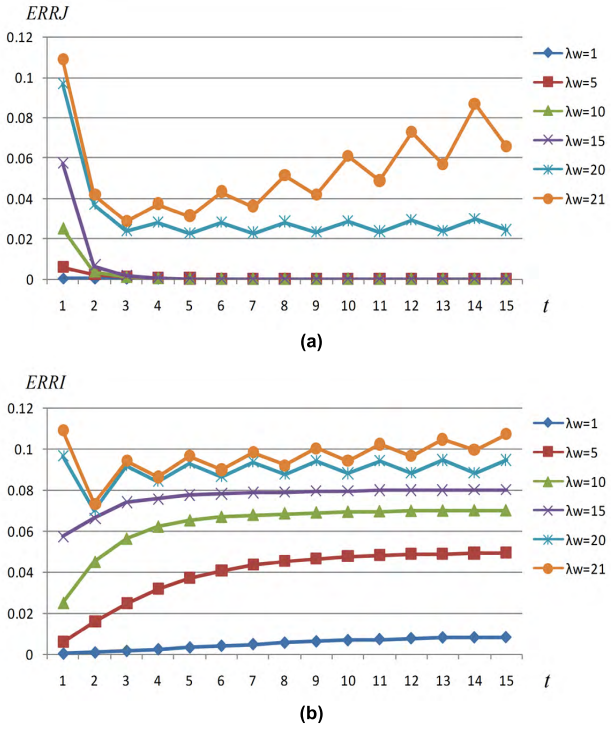

FIGURE 5. The influence of the tuning parameter λ_W and the iterations t for the results obtained from our ATGV-CT method in Fig. 3. (a) (resp. (b)) shows the curves of *ERRJ* (resp. *ERRI*) of the color transfer with our ATGV-CT method in Fig. 3, for different choices of λ_W with t increasing.

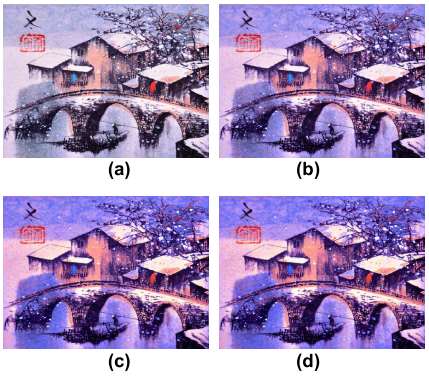

FIGURE 6. The comparison of the color transfer results obtained from model (8) with different λ_W. (a)~(d) correspond to $\lambda_W = 1$, 5, 10 and 15, respectively.

It demonstrates that relatively larger $\lambda_W (\lambda_W \leq 15)$ can obtain good color transfer results. Meanwhile, we also notice that the effects of color transfer of (c) and (d) are relatively good, and the differences between (c) and (d) are not notable in vision. Therefore, in this experiment we can simply set $\lambda_W = 10$ or 15.

B. TYPICAL COLOR TRANSFER RESULTS

As mentioned in Section I, our ATGV-CT method is designed for overcoming the two main drawbacks of the TV-CT method. In this section, four typical color transfer results are

used to demonstrate the ability of preserving image details and restraining staircase effect of our ATGV-CT method, respectively.

To manifest the detail-preserving capability of our newly proposed method, we choose some fabric images which contain rich texture details as the target images. Fig. 7 and 8 show two sets of color transfer results with the target images respectively called as ''oval love'' and ''temptation of line.'' Here, the sizes of the images are 500 × 500, and the fabric images are from the GAMA lab in the Hong Kong Polytechnic University. In Fig. 7 and 8, (a) (resp. (b)) is the source image (resp. the target image), (c) (resp. (d) and (e)) is the resulting image obtained from the TV-CT method (resp. the OTGV-CT method and our ATGV-CT method), and (f) (resp. (g), (h) and (i)) is the local enlarged part of (b) (resp. (c), (d) and (e)).

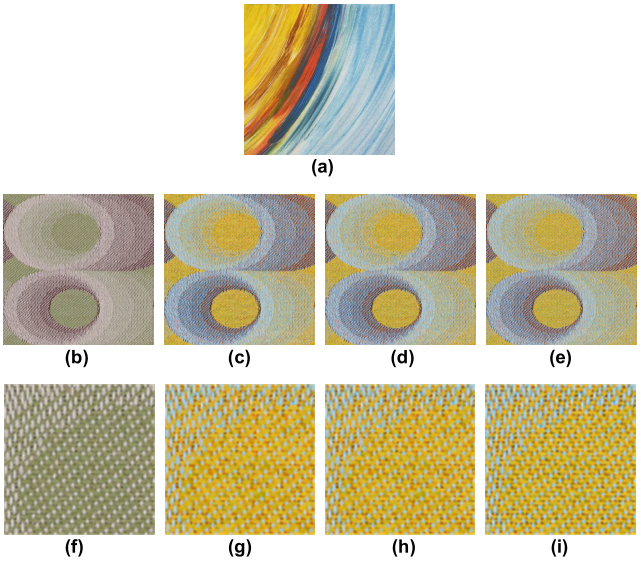

FIGURE 7. The color transfer results with the target image called as "oval love." (a) and (b) are the source image and the target image, respectively, (c) (resp. (d) and (e)) is the resulting image obtained from the TV-CT method (resp. the OTGV-CT method and our newly proposed ATGV-CT method), and (f) (resp. (g), (h) and (i)) is the local enlarged part of (b) (resp. (c), (d) and (e)).

From the results shown in Fig. 7 and 8, we can find that the resulting images obtained from our ATGV-CT method are better than those obtained from the TV-CT method and the OTGV-CT method. As a matter of fact, comparing with the corresponding scene in Fig. 7 (f) (resp. Fig. 8 (f)), we notice that some important texture details are relatively fuzzy in Fig. 7 (g) (resp. Fig. 8 (g)). In some ways, the fuzzy phenomenon of the resulting images obtained from the OTGV-CT method (shown in Fig. 7 (h) and Fig. 8 (h)) are somewhat mitigated but still exist. By contrast, the texture details of the original target images are preserved well in the resulting images obtained from our ATGV-CT method (shown in Fig. 7 (i) and Fig. 8 (i)). It demonstrates that, under the guidance of the adaptive edge indicator, our ATGV-CT method can better preserve the geometrical structure details

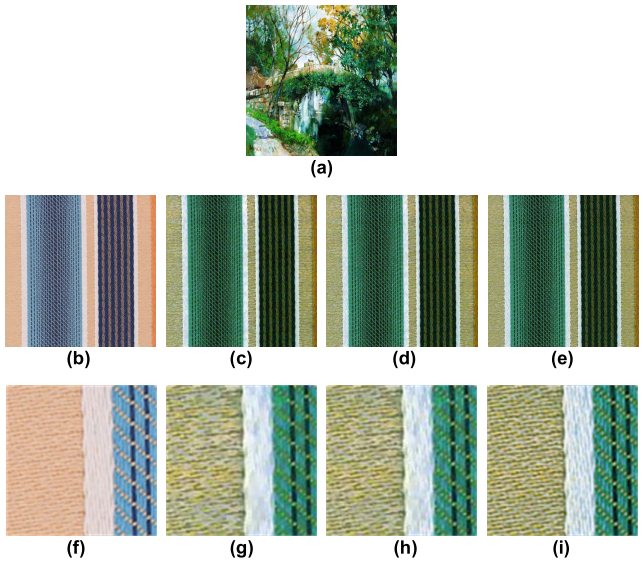

FIGURE 8. The color transfer results with the target image called as "temptation of line." (a) and (b) are the source image and the target image, respectively, (c) (resp. (d) and (e)) is the resulting image obtained from the TV-CT method (resp. the OTGV-CT method and our newly proposed ATGV-CT method), and (f) (resp. (g), (h) and (i)) is the local enlarged part of (b) (resp. (c), (d) and (e)).

of the original target image than the TV-CT method and the OTGV-CT method.

To evaluate the staircase effect inhibition performance of our new method, we choose some images which contain rich smooth regions as the target images. Fig. 9 and 10 show other two sets of color transfer results with the target images respectively called as ''terraced landscape'' and ''sky of city.'' Here, the sizes of the images are 600 × 400. In Fig. 9 and 10, (a) (resp. (b)) is the source image (resp. the target image), (c) (resp. (d)) is the resulting image obtained from the TV-CT method (resp. our ATGV-CT method), and (e) (resp. (f) and (g)) is the local enlarged part of (b) (resp. (c) and (d)).

From observation, we noticed that some staircase effect can be easily found in the resulting images obtained from the TV-CT method (shown in Fig. 9 (f) and Fig. 10 (f)), while the resulting images obtained from our ATGV-CT method (shown in Fig. 9 (g) and Fig. 10 (g)) have not obvious staircase effect. Apparently, compared with the TV-CT method, our new method can obtains better results since the resulting images obtained from our ATGV-CT method are more natural and realistic. In fact, due to the use of the TGV regularizer rather than the TV regularizer, our ATGV-CT method can better restrain the staircase effect.

The color transfer results shown in Fig. 3, 4, 7, 8, 9 and 10 prove that our newly proposed ATGV-CT method can generate better results than the TV-CT method in the aspects of the inhibition of staircase effect and the preservation of image details.

In order to further demonstrate the effectiveness of our proposed ATGV-CT method, the results of a user study test [46] are shown in Table 1. Here, 20 participants are asked to view

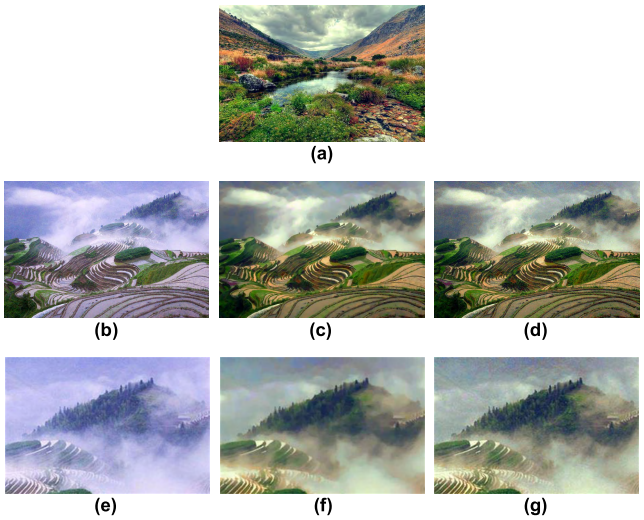

FIGURE 9. The color transfer results with the target image called as "terraced landscape." (a) and (b) are the source image and the target image, respectively, (c) (resp. (d)) is the resulting image obtained from the TV-CT method (resp. our newly proposed ATGV-CT method), and (e) (resp. (f) and (g)) is the local enlarged part of (b) (resp. (c) and (d)).

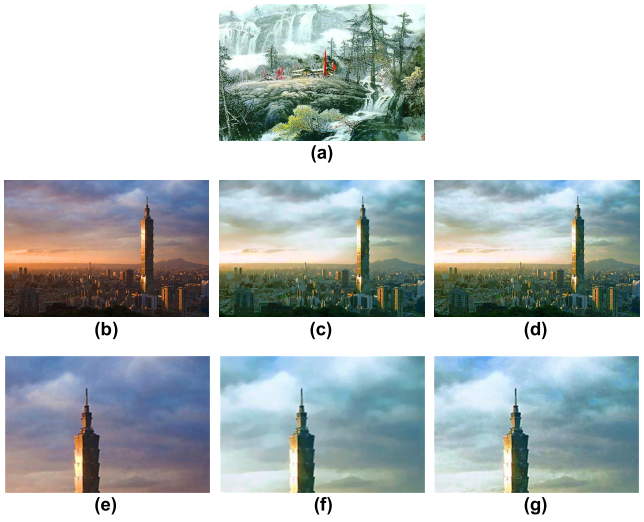

FIGURE 10. The color transfer results with the target image called as "sky of city." (a) and (b) are the source image and the target image, respectively, (c) (resp. (d)) is the resulting image obtained from the TV-CT method (resp. our newly proposed ATGV-CT method), and (e) (resp. (f) and (g)) is the local enlarged part of (b) (resp. (c) and (d)).

10 sets of color transfer results obtained by different methods and give subjective scores with a range of 1-10, where higher the average score better the image quality. Note that the final scores are averaged over all participants and all color transfer results. Moreover, the source of the color transfer results is unknown to the participants and the orders of the color transfer results are randomly placed. From Table 1, it is obvious that the color transfer results obtained by our proposed ATGV-CT method have higher quality.

In addition, Table 2 shows the averaged time statistics of above 10 sets of color transfer results obtained by different methods. From Table 2, the averaged time of our proposed ATGV-CT method is slightly longer than the TV-CT method and the OTGV-CT method. This is mainly because that it needs to spend more time to compute the adaptive TGV regularizer than the TV regularizer and the original TGV regularizer. Considering the time difference is not significant, we believe that the complexity of above three methods belong to the same level, while our proposed ATGV-CT method can obtain better color transfer results.

TABLE 1. User test results for different color transfer methods.

Method	TV-CT	OTGV-CT	ATGV-CT
Average Score	7.95	8.65	9.15

TABLE 2. Timing statistics for different color transfer methods.

Method	TV-CT	OTGV-CT	ATGV-CT
Average Time	96.76s	116.61s	118.28s

V. CONCLUSION

In this paper, we present a new global color transfer method which is called as the ATGV-CT method. Aimed at dealing with the defects of traditional TV regularizer based color transfer methods, an adaptive TGV regularizer is introduced in our new method. Compared with the classical TV-CT method, our newly proposed method can better restrain the staircase effect and preserve the geometrical structure details of the original target images. To solve our newly proposed model, we design an efficient numerical algorithm which combines the former-backward operator splitting method and the weighted primal-dual method. The numerical experiment results show that the resulting images obtained from our newly proposed ATGV-CT method are more realistic and clear than ones obtained from the classical TV-CT method.

ACKNOWLEDGMENT

The authors would like to thank anonymous reviewers for their kind and constructive comments.

REFERENCES

[1] E. Reinhard, M. Adhikhmin, B. Gooch, and P. Shirley, "Color transfer between images," *IEEE Comput. Graph. Appl.*, vol. 21, no. 5, pp. 34–41, Sep./Oct. 2001.
[2] A. Levin, D. Lischinski, and Y. Weiss, "Colorization using optimization," *ACM Trans. Graph.*, vol. 23, no. 3, pp. 689–694, Mar. 2004.
[3] Y.-W. Tai, J. Jia, and C.-K. Tang, "Local color transfer via probabilistic segmentation by expectation-maximization," in *Proc. IEEE Conf. Comput. Vis. Pattern Recognit. (CVPR)*, San Diego, CA, USA, Jun. 2005, pp. 747–754.
[4] H. Chang, O. Fried, Y. Liu, S. DiVerdi, and A. Finkelstein, "Palette-based photo recoloring," *ACM Trans. Graph.*, vol. 34, no. 4, Apr. 2015, Art. no. 139.

[5] Y. Han, C. Xu, G. Baciu, M. Li, and M. R. Islam, "Cartoon and texture decomposition-based color transfer for fabric images," *IEEE Trans. Multimedia*, vol. 19, no. 1, pp. 80–92, Jan. 2017.
[6] Y. Yang, H. Zhao, L. You, R. Tu, X. Wu, and X. Jin, "Semantic portrait color transfer with Internet images," *Multimed. Tools Appl.*, vol. 76, no. 1, pp. 523–541, Jan. 2017.
[7] B. Arbelot, R. Vergne, T. Hurtut, and J. Thollot, "Local texture-based color transfer and colorization," *Comput. Graph.*, vol. 62, pp. 15–27, Feb. 2016.
[8] Z. Yan, H. Zhang, B. Wang, S. Paris, and Y. Yu, "Automatic photo adjustment using deep neural networks," *ACM Trans. Graph.*, vol. 35, no. 2, May 2016, Art. no. 11.
[9] L. A. Gatys, A. S. Ecker, and M. Bethge, "Image style transfer using convolutional neural networks," in *Proc. IEEE Conf. Comput. Vis. Pattern Recognit. (CVPR)*, Las Vegas, NV, USA, Jun. 2016, pp. 2414–2423.
[10] A. Selim, M. Elgharib, and L. Doyle, "Painting style transfer for head portraits using convolutional neural networks," *ACM Trans. Graph.*, vol. 35, no. 4, Jul. 2016, Art. no. 129.
[11] L. He, H. Qi, and R. Zaretzki, "Image color transfer to evoke different emotions based on color combinations," *Signal Image. Video Process.*, vol. 9, no. 8, pp. 1965–1973, Aug. 2015.
[12] C. Ueda, T. Azetsu, N. Suetake, and E. Uchino, "Color transfer method preserving perceived lightness," *Opt. Rev.*, vol. 23, no. 3, pp. 470–478, Mar. 2016.
[13] T. Welsh, M. Ashikhmin, and K. Mueller, "Transferring color to greyscale images," *ACM Trans. Graph.*, vol. 21, no. 3, pp. 277–280, Mar. 2002.
[14] X. Xiao and L. Ma, "Color transfer in correlated color space," in *Proc. ACM Int. Conf. (VRCAI)*, Hong Kong, 2006, pp. 305–309.
[15] N. Xu, W. Lin, Y. Zhou, Y. Chen, Z. Chen, and H. Li, "A new global-based video enhancement algorithm by fusing features of multiple region-of-interests," in *Proc. IEEE Int. Conf. VCIP*, Tainan, Taiwan, Nov. 2011, pp. 1–4.
[16] Y. Chen, W. Lin, C. Zhang, Z. Chen, N. Xu, and J. Xie, "Intra-and-inter-constraint-based video enhancement based on piecewise tone mapping," *IEEE Trans. Circuits Syst. Video Technol.*, vol. 23, no. 1, pp. 74–82, Jan. 2013.
[17] M. Sun, Z. Liu, J. Qiu, Z. Zhang, and M. Sinclair, "Active lighting for video conferencing," *IEEE Trans. Circuits Syst. Video Technol.*, vol. 19, no. 12, pp. 1819–1829, Dec. 2009.
[18] W.-W. Wang, P.-L. Shui, and X.-C. Feng, "Variational models for fusion and denoising of multifocus images," *IEEE Signal Process. Lett.*, vol. 15, no. 1, pp. 65–68, Jan. 2008.
[19] H. Liu, J. Gu, M. Q.-H. Meng, and W.-S. Lu, "Fast weighted total variation regularization algorithm for blur identification and image restoration," *IEEE Access*, vol. 4, pp. 6792–6801, Jan. 2016.
[20] J. Rabin, J. Delon, and Y. Gousseau, "Regularization of transportation maps for color and contrast transfer," in *Proc. IEEE Int. Conf. Image Process.*, Hong Kong, Sep. 2010, pp. 1933–1936.
[21] N. Papadakis, E. Provenzi, and V. Caselles, "A variational model for histogram transfer of color images," *IEEE Trans. Image Process.*, vol. 20, no. 6, pp. 1682–1695, Jun. 2011.
[22] J. Rabin and G. Peyré, "Wasserstein regularization of imaging problem," in *Proc. IEEE Int. Conf. Image Process.*, Brussels, Belgium, Sep. 2011, pp. 1541–1544.
[23] W. Feng, Y. Guo, O. Kim, Y. Hou, L. Liu, and H. Sun, "Color transfer based on earth mover's distance and color categorization," in *Proc. Int. Conf. Comput. Anal. Images Patterns (CAIP)*, York, PA, USA, 2013, pp. 394–401.
[24] A. Bugeau, V.-T. Ta, and N. Papadakis, "Variational exemplar-based image colorization," *IEEE Trans. Image Process.*, vol. 23, no. 1, pp. 298–307, Jan. 2014.
[25] W. Zuo and Z. Lin, "A generalized accelerated proximal gradient approach for total-variation-based image restoration," *IEEE Trans. Image Process.*, vol. 20, no. 10, pp. 2748–2759, Oct. 2011.
[26] X. Li, F. Arroyo, J. Zhu, and J. Sun, "Semisoft generalized total variation minimization for image reconstruction in computed tomography," *IEEE Access*, vol. 5, pp. 8475–8481, Apr. 2017.
[27] D. Tian, D. Y. Xue, and D. H. Wang, "A fractional-order adaptive regularization primal–dual algorithm for image denoising," *Inf. Sci.*, vol. 296, no. 5, pp. 147–159, Mar. 2015.
[28] C. He, C. Hu, X. Yang, H. He, and Q. Zhang, "An adaptive total generalized variation model with augmented lagrangian method for image denoising," *Math. Problems Eng.*, vol. 2014, no. 1, Jan. 2014, Art. no. 157893.
[29] Y. Han, C. Xu, G. Baciu, and X. Feng, "Multiplicative noise removal combining a total variation regularizer and a nonconvex regularizer," *Int. J Comput. Math.*, vol. 91, no. 10, pp. 2243–2259, Oct. 2014.
[30] Y. Wu and X. Feng, "Speckle noise reduction via nonconvex high total variation approach," *Math. Problems Eng.*, vol. 2015, no. 2, Feb. 2015, Art. no. 627417.
[31] K. Bredies, K. Kunisch, and T. Pock, "Total generalized variation," *SIAM J. Imag. Sci.*, vol. 3, no. 3, pp. 492–526, Sep. 2010.
[32] X.-D. Wang, X.-C. Feng, W.-W. Wang, and W.-J. Zhang, "Iterative reweighted total generalized variation based Poisson noise removal model," *Appl. Math. Comput.*, vol. 223, pp. 264–277, Oct. 2013.
[33] T. Valkonen, K. Bredies, and F. Knoll, "Image decomposition and staircase effect reduction based on total generalized variation," *SIAM J. Imag. Sci.*, vol. 6, no. 6, pp. 487–525, Jun. 2013.
[34] F. Knoll, K. Bredies, T. Pock, and R. Stollberger, "Second order total generalized variation (TGV) for MRI," *Magn. Reson. Med.*, vol. 65, no. 2, pp. 480–491, Feb. 2011.
[35] M. T. Qiao, W. Wang, and N. Michael, "Multi-phase texture segmentation using Gabor features histograms based on wasserstein distance," *Comput. Graph. Forum*, vol. 15, no. 5, pp. 1480–1500, May 2014.
[36] L. Wang, L. Xiao, H. Liu, and Z. Wei, "Local brightness adaptive image colour enhancement with Wasserstein distance," *IET Image Process.*, vol. 9, no. 1, pp. 43–53, 2015.
[37] J. Duan *et al.*, "Denoising optical coherence tomography using second order total generalized variation decomposition," *Biomed. Signal Proces.*, vol. 24, no. 2, pp. 120–127, Feb. 2016.
[38] J. Xu, X. Feng, Y. Hao, and Y. Han, "Image decomposition using adaptive second-order total generalized variation," *Signal, Image. Video Process.*, vol. 8, no. 1, pp. 39–47, Jan. 2014.
[39] P. L. Combettes and V. R. Wajs, "Signal recovery by proximal forward-backward splitting," *Multiscale Model. Simul.*, vol. 4, no. 4, pp. 1168–1200, Apr. 2005.
[40] A. Chambolle and T. Pock, "A first-order primal-dual algorithm for convex problems with applications to imaging," *J. Math. Imag. Vis.*, vol. 40, no. 1, pp. 120–145, 2011.
[41] C. He, C. Hu, X. Li, and W. Zhang, "A parallel primal-dual splitting method for image restoration," *Magn. Reson. Med.*, vol. 358, no. 9, pp. 73–91, Sep. 2016.
[42] X. Wang, Y. Bi, X. Feng, and L. G. Huo, "Multiplicative noise removal using primal–dual and reweighted alternating minimization," *SpringerPlus*, vol. 5, no. 1, p. 277, Jan. 2016.
[43] G. Yu, W. Xue, and Y. Zhou, "A nonmonotone adaptive projected gradient method for primal–dual total variation image restoration," *Signal Process.*, vol. 103, pp. 242–249, Oct. 2014.
[44] D.-Q. Chen, X.-P. Du, and Y. Zhou, "Primal-dual algorithm based on Gauss-Seidel scheme with application to multiplicative noise removal," *J. Comput. Appl. Math.*, vol. 292, no. 1, pp. 609–622, Jan. 2016.
[45] Y. Hao, J. L. Xu, and J. Bai, "Primal-dual method for the coupled variational model," *Comput. Electr. Eng.*, vol. 40, no. 3, pp. 808–818, Mar. 2014.
[46] X. Han, C. Zhang, W. Lin, M. Xu, B. Sheng, and T. Mei, "Tree-based visualization and optimization for image collection," *IEEE Trans. Cybern.*, vol. 46, no. 6, pp. 1286–1300, Jun. 2016.

BIN XIE received the M.S. degree in communication and information system from Huazhong University of Science and Technology, Wuhan, China, in 2006. He is currently working toward the Ph.D. degree at Shenzhen University, Shenzhen, China. His research interests include image processing, computer vision, machine learning, and pattern recognition.

CHEN XU received the M.S. degree in mathematics from Xidian University, Xi'an, China, in 1989 and the Ph.D. degree in mathematics from Xian Jiaotong University, Xi'an, China, in 1992. He is currently a Professor of Mathematics and an Advisor for doctoral students at Shenzhen University, Shenzhen, China. His research interests include information and computational science, analysis and application of wavelet, image processing, and computer vision.

YU HAN received the Ph.D. degree in mathematics from Xidian University, Xi'an, China, in 2013. He was a Research Associate at the GAMA Lab, Department of Computing, The Hong Kong Polytechnic University, Hong Kong, from 2011 to 2015. He is currently a Lecturer of Mathematics at Shenzhen University, Shenzhen, China. His research interests include image processing, computer vision, and pattern recognition.

ROBERT K. F. TENG received the Ph.D. degree in electrical engineering from Purdue University, West Lafayetee, IN, USA, in 1986. He is currently a Professor of Information Engineering at Shenzhen University, Shenzhen, China. His research interests include information and computational science, image processing, and computer vision.